Journal Pre-proof

Electrochemical oxidation of PFOA and PFOS in landfill leachates at low and highly boron-doped diamond electrodes

Mattia Pierpaoli (Formal analysis) (Investigation) (Writing - original draft) (Visualization), Małgorzata Szopińska (Conceptualization) (Investigation) (Writing - original draft), Barbara K. Wilk (Validation) (Investigation), Michał Sobaszek (Methodology) (Investigation) (Writing - original draft), Aneta Łuczkiewicz (Methodology) (Resources) (Writing - review and editing), Robert Bogdanowicz (Methodology) (Resources) (Writing - review and editing) (Supervision), Sylwia Fudala-Książek (Conceptualization) (Formal analysis) (Resources) (Writing - review and editing) (Supervision)

PII:	S0304-3894(20)31592-2
DOI:	https://doi.org/10.1016/j.jhazmat.2020.123606
Reference:	HAZMAT 123606
To appear in:	*Journal of Hazardous Materials*
Received Date:	30 April 2020
Revised Date:	14 July 2020
Accepted Date:	27 July 2020

Please cite this article as: { doi: https://doi.org/

Electrochemical oxidation of PFOA and PFOS in landfill leachates at low and highly boron-doped diamond electrodes

Mattia Pierpaoli[1], Małgorzata Szopińska[2], Barbara K. Wilk[2], Michał Sobaszek[1], Aneta Łuczkiewicz[2], Robert Bogdanowicz[1], Sylwia Fudala-Książek[3]

[1] Department of Metrology and Optoelectronics, Faculty of Electronics, Telecommunication and Informatics, Gdańsk University of Technology, Gdańsk, Poland;

[2] Gdansk University of Technology, Faculty of Civil and Environmental Engineering, Department of Water and Wastewater Technology, 11/12 Narutowicza St., Gdansk 80-233, Poland;

[3] Gdansk University of Technology, Faculty of Civil and Environmental Engineering, Department of Sanitary Engineering, 11/12 Narutowicza St., Gdansk 80-233, Poland;

Graphical abstract

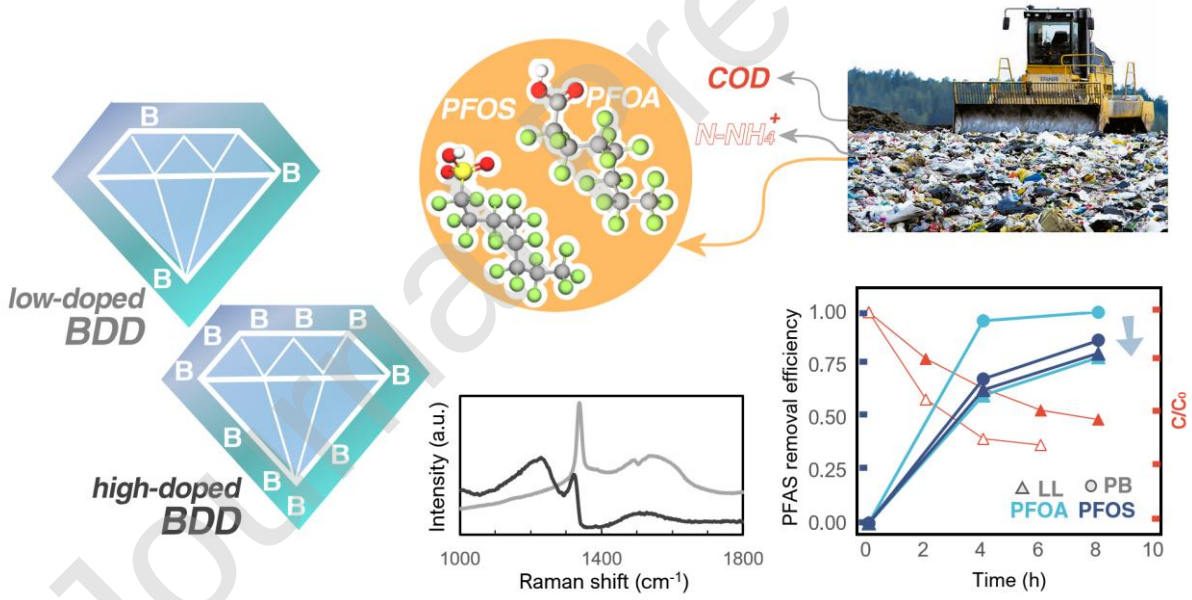

Highlights

- PFOA and PFOS removal from landfill leachate is dependent on current density
- B-doping irrelevantly affects the overall decomposition of PFASs
- PFOS long-chain by-products are more susceptible to electrolysis on 0.5k BDD than 10k BDD
- 0.5k BDD performed COD removal better than the 10k BDD

Abstract

Polyfluorinated alkyl substances (PFASs) may reach landfill leachates (LLs) due to improper waste management. In this study perfluorooctanoate (PFOA) and perfluorooctane sulphonate (PFOS) were used as representatives of PFASs in the decomposition on boron-doped diamond electrodes (BDDs) with high (10k ppm) and low (0.5k ppm) boron doping concentrations. The result shows that although better COD removal efficacies are obtained on the low-doped BDD (59% after 8h), the decomposition rate of PFOA and PFOS was not affected by boron doping. In LLs, at the current density of 75 mA/cm², averaged removal efficiencies of 80% and 78% were achieved for PFOA and PFOS, respectively. But besides concentration of mother compounds, the presence of intermediates during electrolysis should be monitored. After 8 h of LL electrolysis, the presence of long-chain degradates C_6F_{13} and $C_6F_{13}COO^-$ was still observed only in 10k BDD-PFOA assays, while during 0.5k assays C_{6F13} and $C_6F_{13}COO^-$ form more intesively at the beginning of the process. This indirectly confirms the more intensive generation of perfluoroalkoxy and hydroxyl radicals and higher susceptibility to electrolysis of PFOA's long-chain intermediates on 0.5k BDD. This is the first study reporting BDD-electrolysis as promising in PFAS removal from the complex matrix of LLs, despite the oxidation of competing LLs components.

Keywords

Micropollution, PFAS, BDD, Advanced Oxidation Process, degradation efficacy, industrial wastewater

1. Introduction

Polyfluorinated alkyl substances (PFAS) are a group of human-made, widely used, persistent and ubiquitously distributed chemicals. Because of the bioaccumulation of such compounds in the environment, their presence can cause adverse effects in humans. Perfluorooctanoic acid (PFOA), a perfluorocarboxylic acid characterised by at least 8-carbon chain length, and perfluorooctane sulphonate (PFOS), together with their precursors, have attracted the most attention among PFASs as emerging contaminants of global concern.

The main exposure pathways for human are direct, through PFAS presence in consumer goods, and indirect, by their spread in the environment followed by bioaccumulation in the food chain. Perfluorooctane sulphonate adsorption in soil is significant, but smaller than organic compounds of a similar molecular weight (Higgins and Luthy, 2006) . The presence of organic carbon is the dominant parameter affecting sorption on sediments, followed by the presence of Ca_2^+ ions and by decreasing pH, suggesting the

contribution of electrostatic interactions(Johnson et al., 2007).

The primary anthropogenic sources for the release of PFAS into the environment include landfill leachates (Bossi et al., 2008; Trojanowicz et al., 2018), and landfill ambient air may also contain elevated concentrations of PFAS(Hamid et al., 2018). PFOA and PFOS concentration found in landfill leachates have been reported in Table 1.

PFOA and PFOS are persistent in the environment and resistant to typical environmental degradation processes and to most conventional chemical and microbial treatment technologies.

The technologies to remove PFOA and PFOS currently being investigated consist of: adsorption on activated carbon (Deng et al., 2015; Zhang et al., 2016), carbon nanotubes (Deng et al., 2012; Li et al., 2011), polymers (Appleman et al., 2013; Yu et al., 2008), coagulation (Xiao et al., 2013), ion exchange (Deng et al., 2010), micro- and ultra-filtration (Appleman et al., 2013), ball milling (Zhang et al., 2013), constructed wetlands (Yin et al., 2017) and electrochemical oxidation (S. Fudala-Ksiazek et al., 2018; Liao and Farrell, 2009; Pierpaoli et al., 2021; Wang et al., 2020; Zhuo et al., 2012). A non-exhaustive list of the various processes is reported in Table S1, in supporting material.
While many different techniques to remove PFOA and PFOS from aqueous solution have been investigated under controlled environments, the most common and effective installed in leachate treatment plants are reverse osmosis and adsorption on activated carbon (Busch et al., 2010). Biological treatment, air oxidation and nanofiltration are found to be less effective (Yin et al., 2017). However, most of the above-reported techniques require the use of additional chemicals or the production of secondary waste streams.

Among traditional wastewater treatment processes, the electrochemical oxidation process (EO) allows for the effective removal of recalcitrant pollutants, and it presents a few advantages over other conventional process, namely in terms of process effectiveness, energy efficiency, discontinuous operability, small setup size, good scalability and modularity.

PFAS oxidation by EO has been investigated by few authors. While most of the studies are focused on PFOS oxidation in water media, few of them consider more complex effluents, such as industrial wastewater, and the efficiency may largely vary between synthetic electrolytes. The anode material plays an important role in guaranteeing a stable process, as it is subjected to extreme conditions of corrosion (Pierpaoli et al., 2020), without the eventual release of hazardous oxidation by-products.

Electrochemical oxidation of PFAS has been investigated by few authors; in most cases, in water with the addition of an electrolyte. High efficiency together with a high defluorination rate were reached by using both mixed metal oxide and Boron-doped diamond (BDD) electrodes. Zhuo et al. observed the PFOA decomposition occurred through a direct one-electron transfer from the carboxyl group to the Ti/SnO_2-Sb-Bi anode at the potential of 3.37 V (Zhuo et al., 2011). In another study, using a BDD electrode, they reported that at the

potential of 1.5, 2.0 or 2.5V, there was no PFOA degradation. And they linked the lack of activity to the hydroxyl radical, which can be produced from water electrolysis when the potential is higher than the oxygen evolution potential 2.3 V (Zhuo et al., 2012). The importance of the hydroxyl radical in PFOS electrochemical degradation at BDD anode was also highlighted by other authors (Liao and Farrell, 2009; Urtiaga et al., 2015), comparing it to the direct electron transfer process, while many other researchers reported that the hydroxyl radical had a minor effect on the C-F bond. For the water media using different types of anodes (including Ti/SnO_2–Sb, Ti/SnO_2–Sb/PbO_2, Ti/SnO_2–Sb/MnO_2, Ti/SnO_2-Sb-Bi, Ce-PbO_2) a degradation pathway of PFOA is reported and includes mechanisms based on electron transfer, Kolbe decarboxylation, radical reaction, decomposition, and hydrolysis (Liao and Farrell, 2009; Lin et al., 2012; Zhuo et al., 2011, 2012). Therein, direct electron transfer to the anode from the perfluorooctanoate ion and Kolbe decarboxylation reaction occur first at the anode, and are followed by reaction with oxygen, hydroxyl and perfluoroalkoxy radicals (Liao and Farrell, 2009). Removal efficiencies easily reached 90% within three hours of treatment in most cases. Lin and co-workers reached 97% of PFOA degradation in 90 min using a Ti/SnO_2–Sb/Ce–PbO_2 anode (Lin et al., 2013). Moreover, it was found that susceptibility of PFOA to EO was pH-dependent, with the decreasing order of pH 3>pH 9>pH 12 (Urtiaga et al., 2015) and the removal ratio increased with increasing initial PFOA concentration in water solution (Urtiaga et al., 2015). The same trend was observed for F-53B (PFOS substitute) in wastewater (Niu et al., 2012). For some studies EO efficacy for industrial wastewater was performed with the application of BDD resulting in 99.7% PFAS removal (Lin et al., 2012). It is worth highlighting that, despite the PFAS removal rate, monitoring of decomposition species is just as important. However, despite the high efficiency, the main drawback of lead dioxide electrodes is the leaching of toxic ions. For this reason, and for the higher stability, BDD are preferred, as high removal efficiency can be reached.

In this study, for the first time, PFOA and PFOS degradations by electrochemical oxidation on BDD electrode were investigated, in both phosphate buffer and landfill leachate. As real water matrixes are a complex source of pollutants, electrochemical oxidation sees the existence of competing removal mechanisms and the presence of scavenging species, which make it more difficult to efficiently and effectively remove PFOA and PFOS under the same laboratory conditions. For this reason, a thoughtful investigation has been undertaken.

2. Materials and methods

2.1 Landfill leachates

In this study, raw Landfill Leachates (LLs) from a municipal solid waste plant (MSWP) located in the Pomerania region (northern Poland – Central Eastern Europe) were collected. The LLs are gathered by a drainage system at the bottom of the landfill prisms. The MSWP started operating in 2003. From January 2003 till November 2011 it operated with unlimited

disposal of organic wastes (including multi-material packaging or plastics). After November 2011, due to legislative requirements (European Parliament, 1999) directive households were obliged to undertake detailed waste segregation (including green waste), and at the same time the disposal of biodegradable wastes in the modern prism is only partly permitted. What is more, Poland was required to progressively reduce landfilling of biodegradable waste from 80% (1995) to 35% by 2020. Hence, the characteristics of LLs collected from the modern cell (after Nov 2011) and the previous cell (before Nov 2011) differ (Fudala-Ksiazek et al., 2016). In this study LLs from the previous cell were used, because they are characterised by low concentration of total suspended solids, which is desirable for electrolysis (no pre-treatment nor pre-filtration was needed) and their biodegradability is relatively low (Table 2). For electrolysis tests 1:1 (V:V) dilution of raw LLs was used.

High organic concentrations were found in LLs, except for BOD_5 and TSS values, which is typical for the methane phase (Fudala-Ksiazek et al., 2016; Sylwia Fudala-Ksiazek et al., 2018; Renou et al., 2008). The low BOD_5/COD ratio (0.12±0.2), where COD and BOD_5 values were 2687±90 mgO_2/L and 340±45 mg O_2/L, respectively. These results indicate low biodegradability of LLs. The total nitrogen was equal to 1999±92 mg N/L and consisted of mainly ammonia form at the level 1993±87 mg N-NH_4^+/L. The high nitrogen content can be explained by the unlimited disposal of biodegradable waste during the period of the landfill's operation. Phosphorus occurred mainly as P-PO_4^{3-} and accounted for 65%±7% of the TP. In this study, high conductivity was noted, and the presence of chloride and sulphate ions, which is typical in LLs, and has also presented in other works (Kawai et al., 2012; Renou et al., 2008).

The composition of leachates are usually an indicator of waste types and the processes occurring within a variable environment from aerobic to anaerobic and ultimately aerobic. As show in Table 2 the concentrations of PFOA and PFOS are 1350±320 ng/L and 3280±940 ng/L, respectively. Their presence in leachates are affected by the landfilling of mixed waste, including: construction materials, carpets, clothing, electronics, textiles, surfactants, insecticides, etc. (Prevedouros et al., 2006). For comparison, the concentration of PFOA and PFOs presented in the literature range widely from 0.40 ng/L to 9200 ng/L and from 0.01 to 2920 ng/L, respectively (Eggen et al., 2010).

2.2 Boron-doped diamond electrodes (BDDs)

Boron-doped diamond (BDD) are prepared on 2-inch-diameter (50.8-mm) niobium substrates by microwave plasma assisted chemical vapor deposition (MWPECVD) system (SEKI Technotron AX5400S, Japan). Prior to deposition, the substrates are subjected to sand-blasting treatment, cleaned in acetone and isopropanol in an ultrasonic bath, and seeded by spin-coating in a water-based diamond slurry. During deposition, the microwave power and the total pressure are kept at 1300 W and 50 Torr, respectively. The substrate holder temperature is set at 700°C. A gas mixture of H_2, CH_4, and B_2H_6, with a total flow of

328 sccm, has been used for the BDD growth. Flows of B_2H_6 and CH_4 were varied in order to obtain two different boron doping levels ($15 \cdot 10^{17}$ at/cm^3 and $3 \cdot 10^{21}$ at/cm^3).

Scanning electron microscopy (SEM) by Phenom XL using a 10-kV beam accelerating voltage, working in high vacuum mode, equipped with a secondary electron detector (SED), was used to observe the surfaces of the BDD electrodes. Electrochemical properties of the electrode were measured by VMP-300 BioLogic potentiostat, in a three-electrode cell configuration, in which the BDD, a platinum wire and an Ag/AgCl-coated wire served, respectively, as working, counter and reference electrodes. H_2SO_4 0.5M was used as electrolyte.

2.3 Electrochemical oxidation setup

The PFOS was purchased from Dr Ehrenstorfer (LGC standards, purity: 96.4%) and PFOA was purchased from Sigma Aldrich (analytical standard, purity ≥ 98.0%). Stock solution of each, in the concentration of 1g/L was prepared using 100 mg of PFOA/PFOS and dissolved in a 100-ml volumetric flask using purified water (Elix® water, resistivity 15 MΩ•cm at 25°C). For the experiment water, a 100-mM phosphate buffer (PB) solution was used. For this reason 8.7331 g of K_2HPO_4 and 125 µL of 85% H_3PO_4 were dissolved in a 500-ml volumetric flask using purified water. Application of 100 mM phosphate buffer as electrolyte during first stage of experiment allowed to achieve pH similar to the values in landfill leachates and oscillate between 7.03-7.29 (Wang et al., 2020).

The electrochemical experiments were conducted in a specially designed experimental set consisting of a 400-mL undivided electrolytic cell, cooling bath and magnetic stirrer (Electrochemical Stirrer, ES24, Wigo, Poland). The cell contained the BDD electrode as an anode and a stainless steel mesh as a cathode. The anode geometric surface area was 10.5 cm^2. The distance between them was kept constant at about 2.5 cm. All electrochemical oxidation tests were performed under galvanostatic conditions, using a power supply (Gw Instek GPD-2303S). Experiments which allowed for the description of detailed PFOA and PFOS degradation pathways and concentration reduction efficiency during electrolysis using new electrode materials were divided into two parts:

- advanced oxidation process (min. 8 h) provided in water matrix (i.e. 100 mM phosphate buffer solution) with addition of PFOA and PFOS (initial concentration 0.1 mg/L)
- advanced oxidation process (min. 8 h) provided in LLs matrix (1:1 v/v LLs:water solution) with addition of PFOA and PFOS (initial concentration 0.1 mg/L)

A detailed description of research steps is presented in Figure 1.

Each experiment was conducted for eight hours at temperatures maintained at 20–25°C. Nine mL of solution was sampled every two hours for physico-chemical analysis; an additional 10-mL aliquot was taken at 0 h, 4 h and 8 h for micropollutant analysis. Prior to the physico-chemical analysis, the sample was subjected to degassing by mixing on a

multipoint stirrer (Variomag, POLY 15 KOMED, Thermofisher Scientific, USA) at 50 rpm for 10 min.

Determination of chemical oxygen demand (COD), inorganic N compounds ($N\text{-}NH_4^+$, $N\text{-}NO_3^-$, $N\text{-}NO_2^-$, TN), inorganic P compounds ($P\text{-}PO_4^{3-}$, TP), chloride (Cl^-), sulphate (SO_4^{2-}), and sulphides (S^{2-}) was performed using a DR 3900 spectrophotometer (Dr. Lange, GmbH, Germany). Twenty-day biochemical oxygen demand (BOD_{20}) was obtained using the manometric respirometric BOD OxiTop® method. Total suspended solids (TSS), volatile suspended solids (VSS) and mineral suspended solids (MSS) were obtained using the gravimetric method. Parameters such as pH, conductivity and temperature were measured by a portable multi-parameter meter HL-HQ40d (multi, HACH, Germany). The detailed procedure of basic physicochemical analysis is described by S. Fudala-Książek et al. (2018).

To determine the concentrations of selected micro-pollutants during the obtained experiments, ultra-high performance liquid chromatography coupled with mass spectrometry technique (UHPLC-MS, Shimadzu Nexera X2; LC MS-8040) was applied. Electrospray (ESI) was applied due to the small fragmentation that occurs during this type of ionisation (so-called "soft ionisation"). To identify electrochemical oxidation by-products of PFOS and PFOA, the UHPLC-ESI-MS technique was used; however, the analysis was focused on the identification of all ionisable molecules, i.e. all ions were identified using scanning mode (SCAN, m/z range 100–520) – qualitative analysis. Due to the lack of chromophore bonds in PFOA and PFOS, only the MS detector was applied to identify unknown degradation products. During the PFOS and PFOA concentration determinations, the Single Ion Mode (SIM) was applied – quantitative analysis. The chromatographic separation was carried out on Phenomenex Luna Omega Polar (100×2.1 mm; 1.6 µm; C18; 100 Å). Pump A and B were responsible for the chromatographic separation. Mobile phase A was determined to be 2 mM ammonium acetate in water, mobile phase (B) was acetonitrile. Gradient elution was applied: 0min (A=80%, B=20%) then ramp to (A=55%, B=45%) in 7 min, next ramp to (A=80%, B=20%) at 7.1 min and kept till 9.5 min. The column temperature was maintained at 40°C, autosampler temperature at 15°C. The flow rate was 0.4 mL min^{-1}. Regarding MS parameters the nebulising gas (N2), drying gas (N), desolvation temperature, and heat block temperature were set at 3 L min^{-1}, 5 L min^{-1}, 250°C, and 325°C, respectively. All the analytes were determined by Single Ion Monitoring (SIM) in negative ionisation mode: m/z for PFOA was 413.0; and for PFOS 499.0. Advanced Oxidation products were identified using scanning mode (SCAN) under the same chromatographic conditions. The injection volume was dependent on expected/assumed concentrations and ranged between 1 and 5 µL. The method detection limit (MDL) for PFOS and PFOA in aqueous solutions was 0.90 and 0.29 µg/L, respectively, and method quantification limit (MQL): 1.1 µg/L and 0.59 µg/L, respectively.

3. Results and discussion

3.1 BDD characterisation

Figure 2 reports the SEM micrographies, together with the Raman spectra, of the two BDD electrodes used in this study. The different boron doping affects the anode structure and morphology, resulting in different average grain sizes (Figure 2 a–d). Figure 2 e shows Raman spectra recorded at 532 nm for low and high doped diamond electrodes. The BDD 0.5k have an intense diamond peak located at 1332 cm^{-1} and two other visible bands: one is of C-H bending bonds located at 1491 cm^{-1} and the second is a G-band located at 1545 cm^{-1}. The confirmation of high boron doping in the 10k electrode are the strong, wide bands derived from B atoms located at 1216 cm^{-1} and 480 m^{-1} (Bogdanowicz et al., 2013b; Sobaszek et al., 2015). The high incorporation of boron into the diamond lattice results in a shift, in the Raman spectra, of the sp^3 from 1332 cm^{-1} to 1316 cm^{-1} (May et al., 2008; Yu et al., 2013) as well as the presence of the Fano effect (Pruvost and Deneuville, 2001). The G-band is located at 1539 cm^{-1}.

The background current analysis is shown in Figure 3 a. The recorded working potential window is 2.6 V and 3.1 V for 10k and 0.5k electrodes, respectively. The slightly narrower potential window is due to higher carrier concentration in the higher doped electrode (Bogdanowicz et al., 2013a). The EIS spectra (Figure 3 b) includes a semicircular region which represents the electron-transfer-limited process. The impedance spectra have been fitted using the equivalent circuit reported in Figure 3 b insert.
Charge transfer resistances may be converted into exchange current densities (j_0) by the linearised form of the Butler–Volmer equation:

$$j_0 = \frac{RT}{F}\frac{1}{SR_{ct}}$$

where R is the gas constant, F is the Faraday constant, and SR_{ct} is the electrode surface resistance obtained by the EIS model fitting.

Calculated exchange current densities are equal to $6.3 \cdot 10^{-2}$ A/m² and $6.7 \cdot 10^{-2}$ A/m² for the 0.5k an 10k BDD, respectively.

3.2 Electrochemical oxidation tests

In order to oxidise PFOA and PFOS, a minimum potential of 2.0 V and 2.2 V vs. NHE, respectively, should be applied to the anode (Liang et al., 2018). However, a higher applied potential may be necessary to directly transfer electrons from PFOA to the anode, as the hydroxyl radical may be ineffective for PFOA decomposition (Zhuo et al., 2011).

The electrochemical degradations of PFOA and PFOS were evaluated both in phosphate buffer (PB) and landfill leachate, by varying the current density and the anode characteristics.

3.2.1 EO in phosphate buffer

Boron concentration affects the charge carrier mobility within the BDD structure, which impacts the electrical resistivity, the electrode exchange current density and the

electrochemical window. While the sp^3 carbon content, boron doping and surface morphology play a role in the COD and N-NH_4^+ removal efficiency (S. Fudala-Ksiazek et al., 2018), they may be responsible for a different PFOA oxidation rate (Gomez-Ruiz et al., 2019). In contrast, in our study, the PFOA removal ratio for the 0.5k and 10k BDD electrode were comparable, being respectively equal to 89% and 95% after 8 h at the lower specific current (25 mA/cm²) (Figure 4 a). Similarly, the PFOS removal assessed slightly lower, at 84% for BDD 0.5k and 69% for BDD 10k (Figure 4 b).

. The removal ratio of PFOA was faster for the test conducted at higher current (96% after 4 h instead of 62%), resulting in a 99.9% removal after 8 h, against a final 89% (Figure 4a). The removal ratio of PFOS was equal to 84% at 8 h. An increase in the current density did not increase the removal efficiency (Figure 4b).

The higher current density may enhance the direct PFOA and PFOS oxidation through direct electron transfer from the molecule to the anode. However, the full oxidation of PFOA has been reported for lower current densities than 25 mA/cm² (Gomez-Ruiz et al., 2019), which might explain the limited difference between the BDD 0.5k and BDD 10k, for which the PFOA and PFOS degradations are not electron-transfer but mass-transfer limited.

Decomposition products of PFOA and PFOS have been identified in spiked samples of 100-mM phosphate buffer using ESI negative ionisation mode and full range scan of possible molecules. All by-products have been detected after 2 h and 4 h of electrolysis for PFOS and PFOA, respectively. Obtained results are presented in Supplementary Material S2. Moreover, a detailed description of decomposition products (together with intensities of detected signals) obtained during electrolysis in phosphate buffer and LLs is presented in Supplementary Material S3. Proposed structures of identified molecules obtained for electrolysis assays after 4 h using both 0.5k and 10k Ni/BDD are presented in Table 3.

PFOA and PFOS electrochemical degradation has been broadly described in water with the addition of different electrolytes, including NaCl (Zhuo et al., 2020), $NaClO_4$ (Lin et al., 2013; Niu et al., 2012; Urtiaga et al., 2015; Yang et al., 2015; Zhuo et al., 2020, 2012), $NaSO_4$ (Gomez-Ruiz et al., 2019; Zhuo et al., 2020), with a very wide range of conductivity. However, the electrolyte does not only support the charge transfer within the solution, but it may actively play a role in the reaction pathway. While the dissolved chlorine ions from NaCl may produce active chlorine species which strongly participate in the oxidative process, the solvated ClO_4^- is more stable. In case of the presence of Na_2SO_4, sulphate radical may be generated (Panizza and Cerisola, 2008), while phosphate buffer should less affect the micropollutant indirect oxidation.

PFOA pathway

Based on the signals obtained by ESI mass spectrometry (Table 3), the proposed electrochemical degradation reactions (including electron transfer, radicals reaction, Kolbe decarboxylation and hydroxylation) for PFOA anodic degradation are as follows:

At the beginning (Eq. 1) PFOA radical is formed via direct electron transfer from the carboxyl group (one electron loss as direct oxidation).

(1) $C_7F_{15}COO^- \rightarrow C_7F_{15}COO\cdot + e^-$

Next, Kolbe decarboxylation occurred due to high instability of PFOA radical (Eq. 2).

(2) $C_7F_{15}COO\cdot \rightarrow C_7F_{15}\cdot + CO_2$

The $C_7F_{15}\cdot$ radical may react with oxygen as presented in Eq. 3, and next perfluoroheptylperoxy radical may react with another perfluoroalkoxy radical as presented in Eq. 4. Then, decomposition of $C_7F_{15}O\cdot$ to perfluoorohexyl radical and carbonyl fluoride occurs (Eq. 5). Finally, carbonyl fluoride in the hydrolysis reaction produce carbon dioxide and hydrofluoric acid (Eq. 6).

(3) $C_7F_{15}\cdot + O_2 \rightarrow C_7F_{15}OO\cdot$

(4) $C_7F_{15}OO\cdot + R_FCOO\cdot \rightarrow C_7F_{15}O\cdot + R_FCO\cdot + O_2$

(5) $C_7F_{15}O\cdot \rightarrow C_6F_{13}\cdot + COF_2$

(6) $COF_2 + H_2O \rightarrow CO_2 + 2HF$

Perfluoorohеptyl radical ($C_6F_{13}\cdot$) and other radicals of this type (with the reduced n number of CF_2) may undergo hydroxylation (Eq. 7) and, next, intramolecular rearrangement for defluorination (Eq. 8) followed by hydrolysis for defluorination (Eq. 9).

(7) $C_6F_{13}\cdot + \cdot OH \rightarrow C_6F_{13}OH$

(8) $C_6F_{13}OH \rightarrow C_6F_{11}OF + HF$

(9) $C_6F_{11}OF + H_2O \rightarrow C_5F_{11}COO^- + H^+ + HF$

Considering CF_2 unzipping cycle (Eq. 3–5), the identified ions: $C_5F_{11}COO^-$ (m/z = 313), $C_4F_9COO^-$ (m/z = 263), $C_3F_7COO^-$ (m/z = 213) and $C_2F_5COO^-$ (m/z = 163) was formed undergoing the presented mechanism (Eq. 7–9). A similar degradation pathway was also observed by other authors (Lin et al., 2012, 2013; Liu et al., 2019; Zhuo et al., 2011) using different DSA and BDD anodes.

PFOS pathway

Observed ESI mass spectrometry signals (supplementary materials) led us to propose electrochemical degradation reactions including radicals reaction, Kolbe decarboxylation, hydrolysis and hydroxylation for PFOS anodic degradation as follows:

The elimination of two fluoride ions giving the observed $C_8F_{15}SO_3^-$ may be a result of consecutive radical reactions according to equations 10–13.

(10) $C_8F_{17}SO_3^- + \cdot H \rightarrow C_8HF_{16}SO_3^- + F^- + e^-$

(11) $C_8HF_{16}SO_3^- + \cdot OH \rightarrow \cdot C_8F_{16}SO_3^- + H_2O$

(12) $\cdot C_8F_{16}SO_3^- + \cdot H \rightarrow C_8HF_{15}SO_3^- + F^-$

(13) $C_8HF_{15}SO_3^- + \cdot OH \rightarrow \cdot C_8F_{15}SO_3^- + H_2O$

At the same time, the $\cdot C_8F_{16}SO_3^-$ radical may also react with hydroxyl radical (Eq. 14–15).

(14) $\cdot C_8F_{16}SO_3^- + \cdot OH \rightarrow HOC_8F_{15}SO_3^- + F^-$

(15) $HOC_8F_{15}SO_3^- + 2F^- \rightarrow FOC_8F_{15}SO_3^- + HF$

However, only after hydrolysis of the formed product ($FOC_8F_{16}SO_3^-$) (Eq. 16) and followed by the Kolbe decarboxylation reaction (Eq. 17) the perfluoroheptyl sulphate radical is observed (m/z = 369, $C_7F_{15}SO_3^-$).

(16) $FOC_8F_{15}SO_3^- + H_2O \rightarrow {}^-OOCC_7F_{15}SO_3^- + 2H^+$

(17) ${}^-OOCC_7F_{15}SO_3^- \rightarrow C_7F_{15}SO_3^- + CO_2$

The perfluoroocta sulphate radical may react with oxygen, and next with some perfluoroalkoxy radical as in Eq. 18–19 producing $C_7F_{15}SO_3^-$.

(18) $\cdot C_8F_{15}SO_3^- + O_2 \rightarrow \cdot OOC\text{-}C_7F_{15}SO_3^-$

(19) $\cdot OOC_8F_{15}SO_3^- + R_FCOO\cdot \rightarrow \cdot OC_8F_{15}SO_3^- + R_FCO\cdot + O_2$

Then, decomposition of $\cdot OC_8F_{17}SO_3^-$ to perfluorohexyl sulphate radical and carbonyl fluoride occurs (Eq. 20) producing $\cdot C_7F_{15}SO_3^-$ (m/z = 399). Finally, carbonyl fluoride in the hydrolysis reaction produces carbon dioxide and hydrofluoric acid (Eq. 21).

(20) $\cdot OC_8F_{15}SO_3^- \rightarrow \cdot C_7F_{15}SO_3^- + COF_2$

(21) $COF_2 + H_2O \rightarrow CO_2 + 2HF$

Moreover, the perfluorohexyl sulphate radical may hydrolyse to a perfluorohexyl radical (Eq. 22).

(22) $\cdot C_7F_{15}SO_3^- + H_2O \rightarrow C_7F_{15}\cdot + SO_4^{2-} + 2H^+$

On the mass spectra $C_6F_{13}COO^-$ (m/z = 363), $C_5F_{11}COO^-$ (m/z = 313) and $C_4F_9COO^-$ (m/z = 263) was observed. Their formation has already been presented in Eq. 7–9. The reaction pathway has been reported in Figure 5.

Considering the intensity of the registered ESI MS signals (see Table 3) in LLs, PFOS decomposition is acting in a similar way for 0.5k Nb/BDD as for 10k Nb/BDD electrolysis. However, for PFOA it is observed that during electrolysis, where a 0.5k Nb/BDD electrode is applied, formation of $C_6F_{13}\cdot$ and $C_6F_{13}COO^-$ occurs more intensively at the beginning of the

process. The opposite situation is observed for 10k Nb/BDD, where those species are still present in the solution after 8 h with the relatively high intensity (in comparison to the 0.5k electrode), which means they reluctantly undergo further degradation steps. Looking into the proposed reaction chain (Eq. 1–9), it can be noted that in the case of 0.5k Nb/BDD the electrolysis reaction (Eq. 1–2) starts from the substrate $C_6F_{13}COO^-$, and the subsequent reactions in Eq. 7–9 occur more often early in the process than in the case of 10k. This means that direct electrochemical reaction related with the perfluoroalkoxy radicals and hydroxyl radicals "production" on the electrode occurs more intensively on 0.5 Nb/BDD than on 10k Nb/BDD.

3.2.2 EO in leachate

Landfill leachate (LL) is a complex matrix, rich in refractory compounds, organic pollutants and inorganic ions. While the PFOA and PFOS oxidation in a water, supported by an electrolyte, has been widely investigated, the effectiveness of such technique in more complex water streams has been scarcely reported. Liang and co-workers investigated the removal of PFOA and PFOS by EO from a technological wastewater resulting from the ion exchange resin regeneration (Liang et al., 2018) and they reported a PFOA and PFOS removal of 77.2% and 96.5% within a 17-hr electrochemical oxidation treatment. In real conditions, to reach PFOA and PFOS removal efficiencies comparable to that obtained in laboratory conditions, it is necessary to increase reaction time or energy density, as long as organic matter, scavenging compounds, and inorganic salts interfere in the process. PFOA and PFOS removal. Figure 6 reports the COD and N-NH_4^+ normalized concentration during the EO tests. It is possible to observe that the current density mainly affects the process, while the boron doping slightly affect the efficiency, resulting in a better performance for the lower doping level.
PFOA and PFOS removal in LL are reported in Figure 7. The micropollutant concentration decrease is not particularly correlated to the boron doping of the electrode, but it is evident that, at low current densities (25 mA/cm^2) the removal efficiency is halved, compared to the one determined in PB, under the same experimental conditions. At 25 mA/cm^2 the PFOA removal at 8h are 48% and 41%, respectively, for the 0.5k and 10k BDD, while at 75 mA/cm^2 they are equal to 79% and 81% (Figure 7 a,b). PFOS follows a similar trend, reaching a 35% for the 0.5k and 46% for the 10k, until doubling for the higher current density 80% for 0.5k and 75% for 10k (Figure 7 c,d).

The energy consumption (W, kWhm^{-3}) was calculated by multiplying the specific electrical charge (Q, kAhm^{-3}) and the cell potential (V) (Gomez-Ruiz et al., 2019). The energy consumption required for 80% PFOA and 79% PFOS removal was estimated as 88 and 123 kWh/m^3, respectively, for 0.5k BDD (treatment time 8 h). For 10k BDD, after 8 h of treatment, the energy consumption calculated for the maximum PFOA and PFOS degradation rates (of 81% and 75%, respectively) was 114 and 106 kWh/m^3, respectively (Table 4). Energy consumption depends on many factors, including the type of anode, surface

features, current density and reaction time, and hence it is difficult to compare the obtained data with the literature. According to (Liu et al., 2019; Schaefer et al., 2017), where nanocrystalline BDD was applied, the energy consumption was of 50 kWh/m^3 for 50% removal of PFOA and 190 kWh/m^3 for 50% removal of PFOS (Table 4), which is higher than obtained in our study, considering decomposition rate efficacy, even for water matrix. For the industrial water (Gomez-Ruiz et al., 2017), due to the more complex matrix and very high PFAS removal efficacy (99.74%) energy consumption after 10 h of EO process reach even 256 kWh/m^3.

4. Conclusion

In this study, the electrochemical oxidation of PFOA and PFOS was studied both in phosphate buffer and landfill leachate, in order to investigate the effect of competing species within the micropollutant mineralisation process. It was found that:

- 0.5k and 10k BDD electrodes perform similarly for the removal of high concentrations of PFOA and PFOS both in LL and PB;
- 0.5k BDD performed the COD and NH_4^+ removal better than the 10k;
- In PB, both PFOA and PFOS removal were comparable at lower current density to that at higher current density, ranging from 83 to 99.9%;
- In LL, PFOA and PFOS removal were dependent on current density. At higher current density (75 mA/cm^2) it was possible to obtain an average removal efficiency of 80% and 78% for PFOA and PFOS, respectively. At lower current density (25 mA/cm^2), the efficiencies were halved. This is due to the competing reactions within a complex matrix;
- B-doping does not greatly affect PFAS removal efficiency.

Due to the unique electrochemical properties, extended stability and high selectivity, BDD electrodes demonstrated their versatility for the effective removal of micropollutants, even in heavy contaminated and complex liquid waste, such as landfill leachate. Nevertheless, to comprehensively assess the EO effectiveness and applicability, further research should be supplemented by toxicity assays. As the role of boron incorporation seems to play a secondary role in enhancing the electrooxidative process, further studies are intended to investigate smart assemblies of carbon nanostructures toward a more efficient and sustainable process.

Mattia Pierpaoli: Formal analysis, Investigation, Writing - Original Draft, Visualization
Małgorzata Szopińska: Conceptualization, Investigation, Writing - Original Draft
Barbara K. Wilk: Validation, Investigation
Michał Sobaszek: Methodology, Investigation, Writing - Original Draft
Aneta Łuczkiewicz: Methodology, Resources, Writing - Review & Editing
Robert Bogdanowicz: Methodology, Resources, Writing - Review & Editing, Supervision

Sylwia Fudala-Książek: Conceptualization Formal analysis, Resources, Writing - Review & Editing, Supervision

Declaration of interests

☒ The authors declare that they have no known competing financial interests or personal relationships that could have appeared to influence the work reported in this paper.

Acknowledgements

This research was supported by the Polish National Agency for Academic Exchange (NAWA), under the Ulam program, Agreement no. PPN/ULM/2019/1/00061/DEC/1 (M.Pierpaoli). Authors would like to thank the Regional Fund for Environmental Protection and Water Management in Gdansk (Poland), for financing the project entitled "Effective removal of micropollutants from wastewater using electrochemical oxidation on nanocrystalline diamond anodes (DIAOPS)" no. RX-15/13/2017.

Bibliography

Allred, B.M.K., Lang, J.R., Barlaz, M.A., Field, J.A., 2014. Orthogonal zirconium diol/C18 liquid chromatography-tandem mass spectrometry analysis of poly and perfluoroalkyl substances in landfill leachate. J. Chromatogr. A 1359, 202–211. https://doi.org/10.1016/j.chroma.2014.07.056

Appleman, T.D., Dickenson, E.R.V., Bellona, C., Higgins, C.P., 2013. Nanofiltration and granular activated carbon treatment of perfluoroalkyl acids. J. Hazard. Mater. 260, 740–746. https://doi.org/10.1016/j.jhazmat.2013.06.033

Bogdanowicz, R., Czupryniak, J., Gnyba, M., Ryl, J., Ossowski, T., Sobaszek, M., Siedlecka, E.M., Darowicki, K., 2013a. Amperometric sensing of chemical oxygen demand at glassy carbon and silicon electrodes modified with boron-doped diamond. Sensors Actuators, B Chem. 189, 30–36. https://doi.org/10.1016/j.snb.2012.12.007

Bogdanowicz, R., Fabiańska, A., Golunski, L., Sobaszek, M., Gnyba, M., Ryl, J., Darowicki, K., Ossowski, T., Janssens, S.D., Haenen, K., Siedlecka, E.M., 2013b. Influence of the boron doping level on the electrochemical oxidation of the azo dyes at Si/BDD thin film electrodes. Diam. Relat. Mater. 39, 82–88. https://doi.org/10.1016/J.DIAMOND.2013.08.004

Bossi, R., Strand, J., Sortkjær, O., Larsen, M.M., 2008. Perfluoroalkyl compounds in Danish wastewater treatment plants and aquatic environments. Environ. Int. 34, 443–450. https://doi.org/10.1016/j.envint.2007.10.002

Busch, J., Ahrens, L., Sturm, R., Ebinghaus, R., 2010. Polyfluoroalkyl compounds in landfill leachates. Environ. Pollut. 158, 1467–1471. https://doi.org/10.1016/j.envpol.2009.12.031

Deng, S., Nie, Y., Du, Z., Huang, Q., Meng, P., Wang, B., Huang, J., Yu, G., 2015. Enhanced adsorption of perfluorooctane sulfonate and perfluorooctanoate by bamboo-derived granular activated carbon. J. Hazard. Mater. 282, 150–157. https://doi.org/10.1016/j.jhazmat.2014.03.045

Deng, S., Yu, Q., Huang, J., Yu, G., 2010. Removal of perfluorooctane sulfonate from wastewater by anion exchange resins: Effects of resin properties and solution chemistry. Water Res. 44, 5188–5195. https://doi.org/10.1016/j.watres.2010.06.038

Deng, S., Zhang, Q., Nie, Y., Wei, H., Wang, B., Huang, J., Yu, G., Xing, B., 2012. Sorption mechanisms of perfluorinated compounds on carbon nanotubes. Environ. Pollut. 168, 138–144. https://doi.org/10.1016/j.envpol.2012.03.048

Eggen, T., Moeder, M., Arukwe, A., 2010. Municipal landfill leachates: A significant source for new and emerging pollutants. Sci. Total Environ. 408, 5147–5157. https://doi.org/10.1016/j.scitotenv.2010.07.049

European Parliament, 1999. Council Directive 1999/31/EC of 26 April 1999 on the landfill of waste [WWW Document]. URL https://eur-lex.europa.eu/legal-content/EN/TXT/?uri=CELEX%3A31999L0031 (accessed 6.18.20).

Fick, J., Lindberg, R.H., 2011. Results from the Swedish National Screening Programme 2010. Swedish Environ. Res. Inst. 1–32.

Fudala-Ksiazek, S., Pierpaoli, M., Kulbat, E., Luczkiewicz, A., 2016. A modern solid waste management strategy - the generation of new by-products. Waste Manag. 49, 516–529. https://doi.org/10.1016/j.wasman.2016.01.022

Fudala-Ksiazek, Sylwia, Pierpaoli, M., Luczkiewicz, A., 2018. Efficiency of landfill leachate treatment in a MBR/UF system combined with NF, with a special focus on phthalates and bisphenol A removal. Waste Manag. 78, 94–103. https://doi.org/10.1016/j.wasman.2018.05.012

Fudala-Ksiazek, S., Sobaszek, M., Luczkiewicz, A., Pieczynska, A., Ofiarska, A., Fiszka-Borzyszkowska, A., Sawczak, M., Ficek, M., Bogdanowicz, R., Siedlecka, E.M., 2018. Influence of the boron doping level on the electrochemical oxidation of raw landfill leachates: Advanced pre-treatment prior to the biological nitrogen removal. Chem. Eng. J. 334, 1074–1084. https://doi.org/10.1016/j.cej.2017.09.196

Fuertes, I., Gómez-Lavín, S., Elizalde, M.P., Urtiaga, A., 2017. Perfluorinated alkyl substances (PFASs) in northern Spain municipal solid waste landfill leachates. Chemosphere 168, 399–407. https://doi.org/10.1016/j.chemosphere.2016.10.072

Gomez-Ruiz, B., Diban, N., Urtiaga, A., 2019. Comparison of microcrystalline and ultrananocrystalline boron doped diamond anodes: Influence on perfluorooctanoic acid electrolysis. Sep. Purif. Technol. 208, 169–177. https://doi.org/10.1016/j.seppur.2018.03.044

Gomez-Ruiz, B., Gómez-Lavín, S., Diban, N., Boiteux, V., Colin, A., Dauchy, X., Urtiaga, A., 2017. Efficient electrochemical degradation of poly- and perfluoroalkyl substances (PFASs) from the effluents of an industrial wastewater treatment plant. Chem. Eng. J. 322, 196–204. https://doi.org/10.1016/j.cej.2017.04.040

Hamid, H., Li, L.Y., Grace, J.R., 2018. Review of the fate and transformation of per- and polyfluoroalkyl substances (PFASs) in landfills. Environ. Pollut. https://doi.org/10.1016/j.envpol.2017.12.030

Higgins, C.P., Luthy, R.G., 2006. Sorption of perfluorinated surfactants on sediments. Environ. Sci. Technol. 40, 7251–7256. https://doi.org/10.1021/es061000n

Huset, C.A., Barlaz, M.A., Barofsky, D.F., Field, J.A., 2011. Quantitative determination of fluorochemicals in municipal landfill leachates. Chemosphere 82, 1380–1386. https://doi.org/10.1016/j.chemosphere.2010.11.072

Johnson, R.L., Anschutz, A.J., Smolen, J.M., Simcik, M.F., Penn, R.L., 2007. The Adsorption of Perfluorooctane Sulfonate onto Sand, Clay, and Iron OxideSurfaces 1165–1170.

Kawai, M., Purwanti, I.F., Nagao, N., Slamet, A., Hermana, J., Toda, T., 2012. Seasonal variation in chemical properties and degradability by anaerobic digestion of landfill leachate at Benowo in Surabaya, Indonesia. J. Environ. Manage. 110, 267–275. https://doi.org/10.1016/j.jenvman.2012.06.022

Li, X., Zhao, H., Quan, X., Chen, S., Zhang, Y., Yu, H., 2011. Adsorption of ionizable organic contaminants on multi-walled carbon nanotubes with different oxygen contents. J. Hazard. Mater. 186, 407–415. https://doi.org/10.1016/j.jhazmat.2010.11.012

Liang, S., Pierce, R. "David," Lin, H., Chiang, S.Y.D., Huang, Q. "Jack," 2018. Electrochemical oxidation of PFOA and PFOS in concentrated waste streams. Remediation 28, 127–134. https://doi.org/10.1002/rem.21554

Liao, Z., Farrell, J., 2009. Electrochemical oxidation of perfluorobutane sulfonate using boron-doped diamond film electrodes. J. Appl. Electrochem. 39, 1993–1999. https://doi.org/10.1007/s10800-009-9909-z

Lin, H., Niu, J., Ding, S., Zhang, L., 2012. Electrochemical degradation of perfluorooctanoic acid (PFOA) by Ti/SnO2-Sb, Ti/SnO2-Sb/PbO2 and Ti/SnO2-Sb/MnO2 anodes. Water Res. 46, 2281–2289. https://doi.org/10.1016/j.watres.2012.01.053

Lin, H., Niu, J., Xu, J., Huang, H., Li, D., Yue, Z., Feng, C., 2013. Highly Efficient and Mild Electrochemical Mineralization of Long-Chain Perfluorocarboxylic Acids (C9–C10) by Ti/SnO 2 –Sb–Ce, Ti/SnO 2 –Sb/Ce–PbO 2 , and Ti/BDD Electrodes. Environ. Sci. Technol. 47, 13039–13046. https://doi.org/10.1021/es4034414

Liu, Y., Fan, X., Quan, X., Fan, Y., Chen, S., Zhao, X., 2019. Enhanced Perfluorooctanoic Acid Degradation by Electrochemical Activation of Sulfate Solution on B/N Codoped Diamond. Environ. Sci. Technol. 53, 5195–5201. https://doi.org/10.1021/acs.est.8b06130

May, P.W., Ludlow, W.J., Hannaway, M., Heard, P.J., Smith, J.A., Rosser, K.N., 2008. Raman and conductivity studies of boron-doped microcrystalline diamond, facetted nanocrystalline diamond and cauliflower diamond films. Diam. Relat. Mater. 17, 105–117. https://doi.org/10.1016/j.diamond.2007.11.005

Niu, J., Lin, H., Xu, J., Wu, H., Li, Y., 2012. Electrochemical mineralization of perfluorocarboxylic acids (PFCAs) by Ce-doped modified porous nanocrystalline PbO2 film electrode. Environ. Sci. Technol. 46, 10191–10198. https://doi.org/10.1021/es302148z

Panizza, M., Cerisola, G., 2008. Removal of colour and COD from wastewater containing acid blue 22 by electrochemical oxidation. J. Hazard. Mater. 153, 83–88. https://doi.org/10.1016/j.jhazmat.2007.08.023

Pierpaoli, M., Jakobczyk, P., Sawczak, M., Łuczkiewicz, A., Fudala-Książek, S., Bogdanowicz, R., 2021. Carbon nanoarchitectures as high-performance electrodes for the electrochemical oxidation of landfill leachate. J. Hazard. Mater. 401, 123407. https://doi.org/10.1016/j.jhazmat.2020.123407

Pierpaoli, M., Rycewicz, M., Łuczkiewicz, A., Fudala-Książek, S., Bogdanowicz, R., Ruello, M.L., 2020. Electrodes criticality: the impact of CRMs in the leachate electrochemical oxidation. Manuf. Rev. 7, 7. https://doi.org/10.1051/MFREVIEW/2020006

Prevedouros, K., Cousins, I.T., Buck, R.C., Korzeniowski, S.H., 2006. Sources, fate and transport of perfluorocarboxylates. Environ. Sci. Technol. 40, 32–44. https://doi.org/10.1021/es0512475

Pruvost, F., Deneuville, A., 2001. Analysis of the Fano in diamond. Diam. Relat. Mater. 10, 531–535. https://doi.org/10.1016/S0925-9635(00)00378-2

Renou, S., Givaudan, J.G., Poulain, S., Dirassouyan, F., Moulin, P., 2008. Landfill leachate treatment: Review and opportunity. J. Hazard. Mater. 150, 468–493. https://doi.org/10.1016/j.jhazmat.2007.09.077

Rodriguez-Freire, L., Balachandran, R., Sierra-Alvarez, R., Keswani, M., 2015. Effect of sound frequency and initial concentration on the sonochemical degradation of perfluorooctane sulfonate (PFOS). J. Hazard. Mater. 300, 662–669. https://doi.org/10.1016/j.jhazmat.2015.07.077

Schaefer, C.E., Andaya, C., Burant, A., Condee, C.W., Urtiaga, A., Strathmann, T.J., Higgins, C.P., 2017. Electrochemical treatment of perfluorooctanoic acid and perfluorooctane sulfonate: Insights into mechanisms and application to groundwater treatment. Chem. Eng. J. 317, 424–432. https://doi.org/10.1016/j.cej.2017.02.107

Sobaszek, M., Skowroński, Bogdanowicz, R., Siuzdak, K., Cirocka, A., Zięba, P., Gnyba, M., Naparty, M., Gołuński, Płotka, P., 2015. Optical and electrical properties of ultrathin transparent nanocrystalline boron-doped diamond electrodes. Opt. Mater. (Amst). 42, 24–34. https://doi.org/10.1016/j.optmat.2014.12.014

Trojanowicz, M., Bojanowska-Czajka, A., Bartosiewicz, I., Kulisa, K., 2018. Advanced

Oxidation/Reduction Processes treatment for aqueous perfluorooctanoate (PFOA) and perfluorooctanesulfonate (PFOS) – A review of recent advances. Chem. Eng. J. 336, 170–199. https://doi.org/10.1016/j.cej.2017.10.153

Urtiaga, A., Fernández-González, C., Gómez-Lavín, S., Ortiz, I., 2015. Kinetics of the electrochemical mineralization of perfluorooctanoic acid on ultrananocrystalline boron doped conductive diamond electrodes. Chemosphere 129, 20–26. https://doi.org/10.1016/j.chemosphere.2014.05.090

Wang, Y., Pierce, R. "david," Shi, H., Li, C., Huang, Q., 2020. Electrochemical degradation of perfluoroalkyl acids by titanium suboxide anodes. Environ. Sci. Water Res. Technol. 6, 144–152. https://doi.org/10.1039/c9ew00759h

Xiao, F., Simcik, M.F., Gulliver, J.S., 2013. Mechanisms for removal of perfluorooctane sulfonate (PFOS) and perfluorooctanoate (PFOA) from drinking water by conventional and enhanced coagulation. Water Res. 47, 49–56. https://doi.org/10.1016/j.watres.2012.09.024

Yang, B., Jiang, C., Yu, G., Zhuo, Q., Deng, S., Wu, J., Zhang, H., 2015. Highly efficient electrochemical degradation of perfluorooctanoic acid (PFOA) by F-doped Ti/SnO2 electrode. J. Hazard. Mater. 299, 417–424. https://doi.org/10.1016/j.jhazmat.2015.06.033

Yin, T., Chen, H., Reinhard, M., Yi, X., He, Y., Gin, K.Y.H., 2017. Perfluoroalkyl and polyfluoroalkyl substances removal in a full-scale tropical constructed wetland system treating landfill leachate. Water Res. 125, 418–426. https://doi.org/10.1016/j.watres.2017.08.071

Yu, Q., Deng, S., Yu, G., 2008. Selective removal of perfluorooctane sulfonate from aqueous solution using chitosan-based molecularly imprinted polymer adsorbents. Water Res. 42, 3089–3097. https://doi.org/10.1016/j.watres.2008.02.024

Yu, Z.M., Wang, J., Wei, Q.P., Meng, L.C., Hao, S.M., Long, F., 2013. Preparation, characterization and electrochemical properties of boron-doped diamond films on Nb substrates. Trans. Nonferrous Met. Soc. China (English Ed. 23, 1334–1341. https://doi.org/10.1016/S1003-6326(13)62601-1

Zhang, D., Luo, Q., Gao, B., Chiang, S.Y.D., Woodward, D., Huang, Q., 2016. Sorption of perfluorooctanoic acid, perfluorooctane sulfonate and perfluoroheptanoic acid on granular activated carbon. Chemosphere 144, 2336–2342. https://doi.org/10.1016/j.chemosphere.2015.10.124

Zhang, K., Huang, J., Yu, G., Zhang, Q., Deng, S., Wang, B., 2013. Destruction of Perfluorooctane Sulfonate (PFOS) and Perfluorooctanoic Acid (PFOA) by Ball Milling.

Zhuo, Q., Deng, S., Yang, B., Huang, J., Wang, B., Zhang, T., Yu, G., 2012. Degradation of perfluorinated compounds on a boron-doped diamond electrode. Electrochim. Acta 77, 17–22. https://doi.org/10.1016/j.electacta.2012.04.145

Zhuo, Q., Deng, S., Yang, B., Huang, J., Yu, G., 2011. Efficient electrochemical oxidation of perfluorooctanoate using a Ti/SnO2-Sb-Bi anode. Environ. Sci. Technol. 45, 2973–2979. https://doi.org/10.1021/es1024542

Zhuo, Q., Wang, J., Niu, J., Yang, B., Yang, Y., 2020. Electrochemical oxidation of perfluorooctane sulfonate (PFOS) substitute by modified boron doped diamond (BDD) anodes. Chem. Eng. J. 379, 122280. https://doi.org/10.1016/j.cej.2019.122280

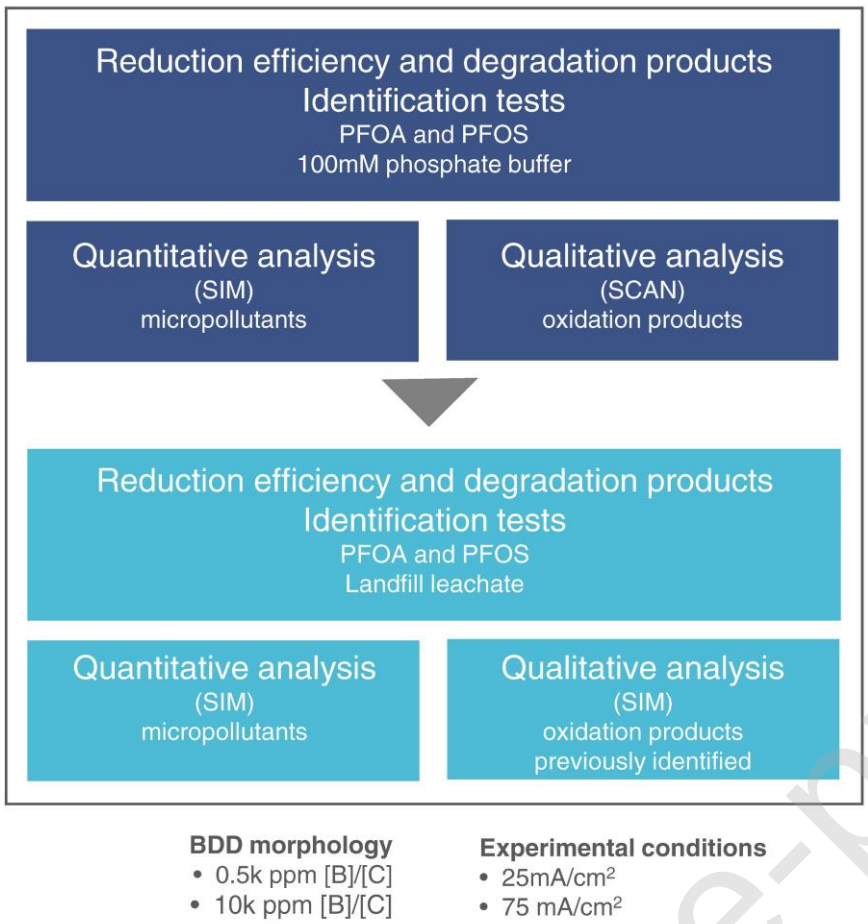

Figure 1 - Operational scheme

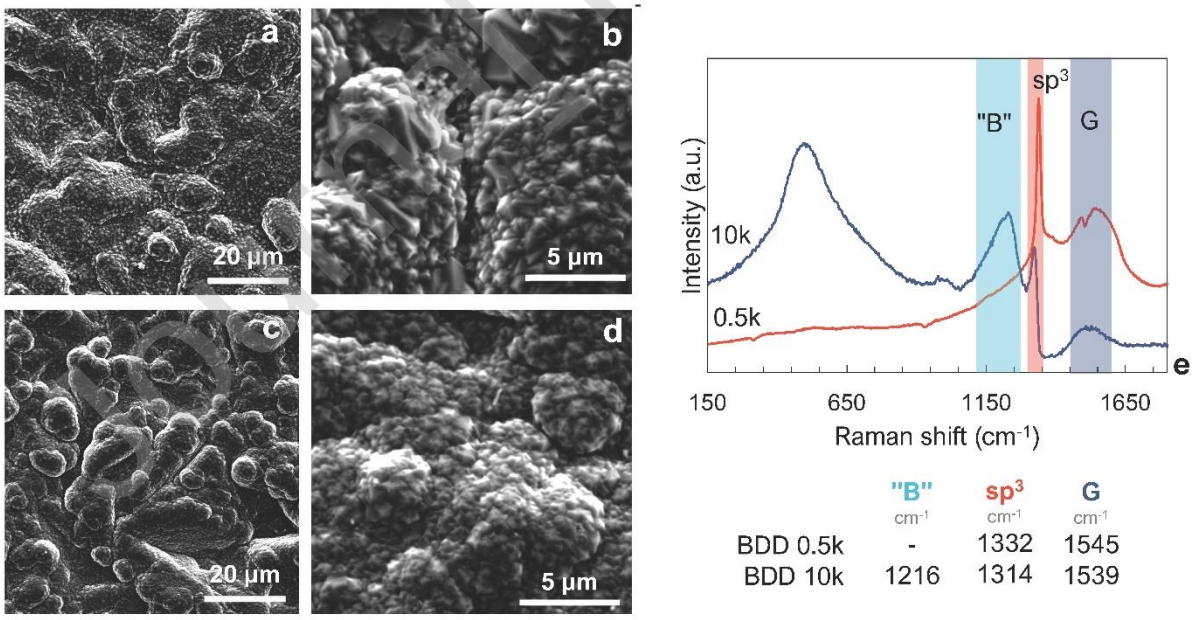

	"B" cm⁻¹	sp³ cm⁻¹	G cm⁻¹
BDD 0.5k	-	1332	1545
BDD 10k	1216	1314	1539

Figure 2 - SEM micrography of the BDD 0.5k (a,b) and BDD 10k (c,d). Raman spectra of the electrodes, with the reported main peak position (e)

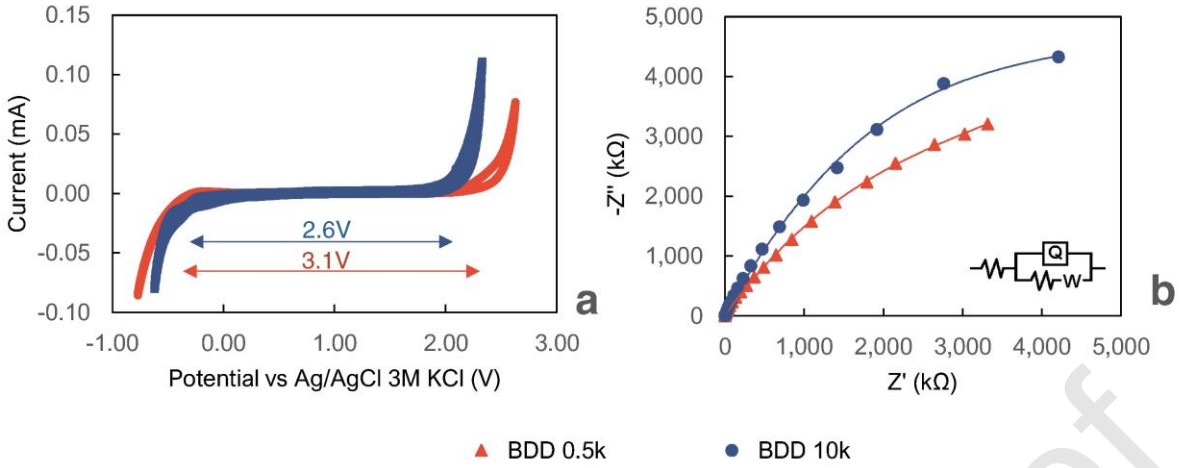

Figure 3 - (a) Cyclic voltammogram of BDD at different B doping (b) electrochemical impedance spectra of the BDD tested in 0.5 m H_2SO_4 as electrolyte vs. Ag/AgCl

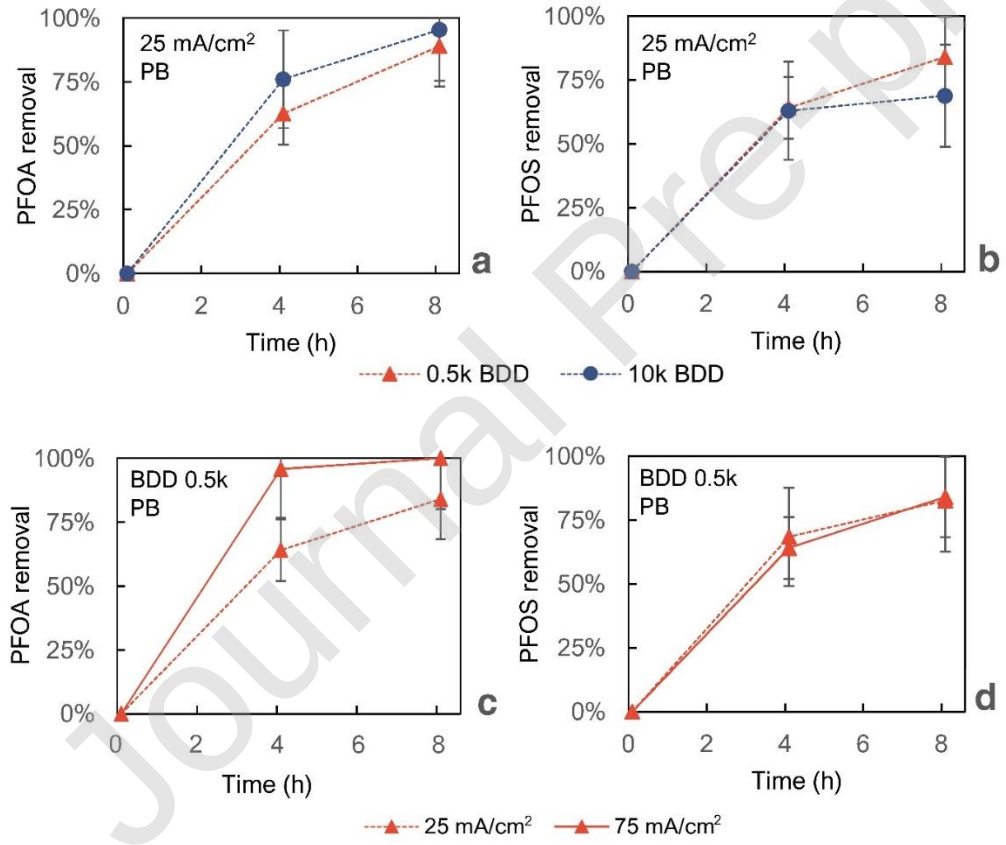

Figure 4 – (a,c) PFOA and (b,d) PFOS removal in PB at low current density (25 mA/cm²) for the 0.5k and 10k BDD anode and for the 0.5k BDD at different current density (25 mA/cm² and 75mA/cm²).

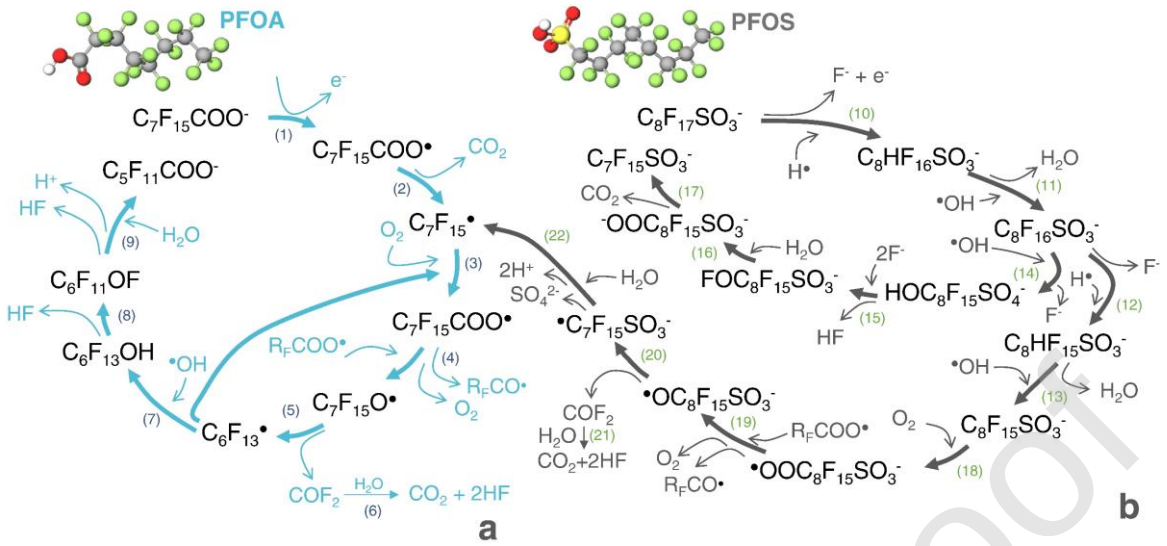

Figure 5 – Proposed reaction pathway for the PFOA and PFOS electrochemical oxidation

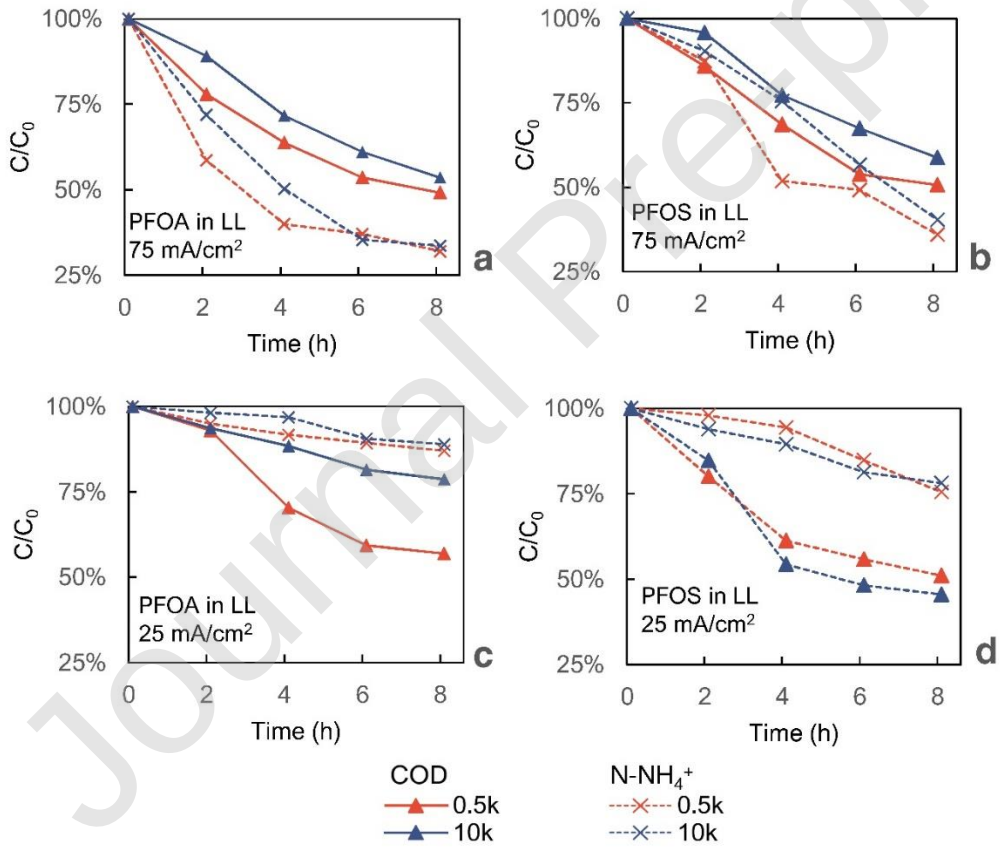

Figure 6 - COD and N-NH_4^+ normalised concentration during LL electrochemical oxidation tests

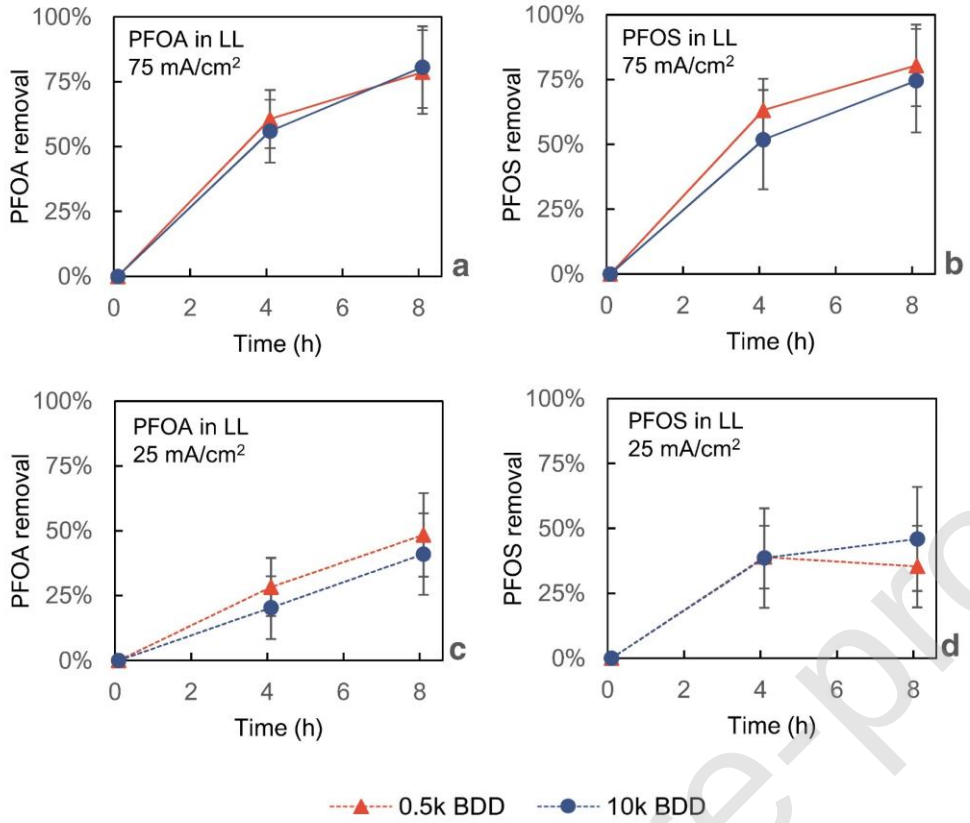

Figure 7 - PFOA and PFOS normalised concentrations for the various EO tests in LL

Table 1 - Occurrence of PFOA and PFOS in landfill leachates

Country	year	PFOA (ng/L)	PFOS (ng/L)	Ref.
U.S..	2014	380–1000	56–160	(Huset et al., 2011)
U.S.	2014	150–9200	14–590	(Allred et al., 2014)
Spain	2017	200–584	0–43.5	(Fuertes et al., 2017)
Germany	2010	0.4–926	0.01–235	(Busch et al., 2010)
Sweden	2010	38–1000	32–1500	(Fick and Lindberg, 2011)
Denmark	2008	2–5.8	1.5–3.8	(Bossi et al., 2008)
Poland	2020	1350	3280	*This study*

Table 2 - Landfill leachates characteristic [mean±SD]

	Parameter	Value
Organic matter characteristics	COD [mg/L]	2867±90
	BOD_{20} [mg/L]	340±45
	BOD_{20}/COD	0.12±0.02
	TSS [mg/L]	80.3±5.7
	MSS [mg/L]	38.0±9.2
	VSS [mg/L]	42.3±7.6
Nitrogen forms	$N\text{-}NH_4^+$ [mg/L]	1993+87
	$N\text{-}NO_3^-$ [mg/L]	13.0±4.5
	$N\text{-}NO_2^-$ [mg/L]	0.33±0.11
	TN [mg/L]	1999±92
Phosphate forms	$P\text{-}PO_4^{3-}$ [mg/L]	9.3±1.2
	TP [mg/L]	14.3±0.53
Other ions	Cl^- [mg/L]	2727±36
	SO_4^{2-} [mg/L]	1106±129
	S^{2-} [mg/L]	9.55±0.46
Basic physicochemical parameters	pH	7.8±0.1
	redox [mV]	-410±0.7
	Conductivity [mS/cm]	23.0±2.8
Selected micropollutants	PFOA [ng/L]	1350±320
	PFOS [ng/L]	3280±940

Table 3 - Suggested structures of molecules identified using negative mode ESI mass spectrometry signals obtained for electrolysis assays after 4 h using both 0.5k and 10k Ni/BDD

Detailed information about degradation products [m/z]								
PFOA; $C_7F_{15}COOH$; m/z =413 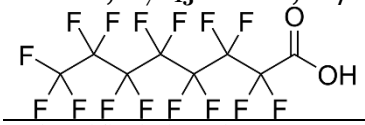								
Identified signals	**369**	**319**	**363**	**313**	**263**	**213**	**163**	**269**
Proposed formula	C_7F_{15}	C_6F_{13}	C_6F_{13} COO^-	C_5F_{11} COO^-	C_4F_9 COO^-	C_3F_7 COO^-	C_3F_7 COO^-	**C_5 F_{11}**
PFOS; $C_8F_{17}HSO_3$; m/z =499 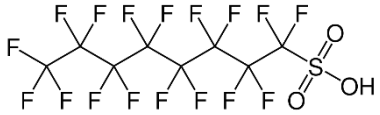								
461	**449**	**399**	**369**	**319**	**363**	**313**	**263**	Identified signals
$C_8F_{15}SO_3^-$	C_7F_{15} SO_3^-	C_6F_{13} SO_3^-	C_7F_{15}	C_6F_{13}	C_6F_{13} COO^-	C_5F_{11} COO^-	C_4F_9 COO^-	Proposed formula

Table 4 - Energy consumption for various parameters of the PFOA and PFOS degradation process

Perfluorinated compounds	Anode	Media	Removal efficiency [%]	Current density [mA/cm²]	Energy consumption [kWh/m³]	Removal time [h]	Ref
PFOA	0.5k BDD	LL	79	75	88	8	This study
PFOA	10k BDD	LL	81	75	114	8	This study
PFAS	BDD	IW	99.74	50	256	10	(Gomez-Ruiz et al., 2017)
PFOA	BDD	GW	50	50	50	8	(Schaefer et al., 2017)
PFOA	BDD	GW	50	15	40	8	(Schaefer et al., 2017)
PFOS	0.5k BDD	LL	80	75	123	8	This study
PFOS	10k BDD	LL	75	75	106	8	This study
PFOS	BDD	GW	50	50	190	8	(Schaefer et al., 2017)
PFOS	BDD	GW	50	15	120	8	(Schaefer et al., 2017)

IW: industrial wastewater; GW: groundwater